

## Article

# Optimization-Design and Atomization-Performance Study of Aerial Dual-Atomization Centrifugal Atomizer

Zhou Yang <sup>1,2,3</sup>, Jiayang Yu <sup>1,2</sup>, Jieli Duan <sup>1,2</sup> , Xing Xu <sup>4,\*</sup>  and Guangsheng Huang <sup>1,2</sup>

<sup>1</sup> College of Engineering, South China Agricultural University, Guangzhou 510642, China

<sup>2</sup> Guangdong Laboratory for Lingnan Modern Agriculture, Guangzhou 510642, China

<sup>3</sup> School of Mechanical Engineering, Guangdong Ocean University, Zhanjiang 524088, China

<sup>4</sup> College of Electronic Engineering (College of Artificial Intelligence), South China Agricultural University, Guangzhou 510642, China

\* Correspondence: xuxing@scau.edu.cn

**Abstract:** The aerial atomizer is the most essential component of the plant protection UAV (unmanned aerial vehicle). However, the structural optimization of existing aerial atomizers lacks comprehensive consideration of spray parameters and structural parameters, and there is a shortage of available atomizer spray models, resulting in the unstable effect of UAV application. In our previous work, an aerial dual-atomization centrifugal atomizer was developed. In order to obtain an aerial atomizer with good atomization effect and its atomization model, structural optimization at different rotation speeds and flow rates of the atomizer, and its atomization performance, are studied in this paper. Firstly, with the droplet volume median diameter (VMD) and spectral width (SRW) as the evaluation index, through the single-factor, Plackett–Burman and Box–Behnken tests, the influence of rotation speed, flow rate, tooth number and tooth shape were studied. The regression models of the droplet VMD and SRW were established using multiple quadratic regression fitting of the test data. Secondly, in order to achieve the lowest droplet VMD and SRW, the response surface method and post-hoc multiple comparison method were used to obtain the optimized structure of the atomizer's rotation ring at different rotation speeds (600–7000 r/min) and flow rates (500–1000 mL/min). Lastly, with the effective swath width (ESW) of the optimized atomizer as the evaluation index, through the Box–Behnken test, the influence of rotation speed, flow rate and spray height were studied. The multiple quadratic regression model of ESW was established with the test data. The test results indicated that rotation speed, flow rate and tooth number had a significant effect on droplet VMD and SRW; tooth shape had no significant effect on the droplet VMD and SRW, however, the square tooth shape had the best atomization effect; and rotation speed, flow rate and spray height had a significant effect on ESW. The optimized structural parameters were tooth shape: square, and tooth number: 20. The determination coefficient  $R^2$  of the regression model of VMD, SRW and ESW were 0.9976, 0.9770 and 0.9974, respectively, which indicates that the model was accurate, and can evaluate and predict the spray effect. This paper provides an optimized dual-atomization centrifugal atomizer, and its regression models of VMD, SRW and ESW for UAV applications can provide a reference for efficient UAV spraying.

**Keywords:** aerial application; centrifugal atomizer; droplet-volume median diameter; droplet spectral width; effective swath width; response surface; regression models



**Citation:** Yang, Z.; Yu, J.; Duan, J.; Xu, X.; Huang, G. Optimization-Design and Atomization-Performance Study of Aerial Dual-Atomization Centrifugal Atomizer. *Agriculture* **2023**, *13*, 430. <https://doi.org/10.3390/agriculture13020430>

Academic Editors: Francisco J. Castillo Ruiz and Francesco Marinello

Received: 28 December 2022

Revised: 5 February 2023

Accepted: 10 February 2023

Published: 11 February 2023



**Copyright:** © 2023 by the authors. Licensee MDPI, Basel, Switzerland. This article is an open access article distributed under the terms and conditions of the Creative Commons Attribution (CC BY) license (<https://creativecommons.org/licenses/by/4.0/>).

## 1. Introduction

The UN Food and Agriculture Organization (FAO) estimates that plant pests and diseases cause 20–40% of crop losses worldwide [1]. Pesticide application is an important tool to control crop pests and diseases. Over the past few decades, with the development of precision agriculture, precision spraying technology has been used to greatly improve the effective utilization of pesticides, which is essential for the prevention and control of pests

and diseases, and meets the demand for green agriculture in current agricultural development [2–4]. Traditional spraying technology mainly includes self-propelled sprayers or knapsack sprayers. Although the former are widely used on field crops for high-efficiency precision spraying, they are difficult to deploy in hills, mountains, paddy fields and other environments with low flexibility, and with low pesticide utilization; the operation process of the latter is very subjective, and its operators are easily exposed to pesticides [5–10]. Crop damage, a reduction in production area and soil compaction are caused by operators walking over or sprayers passing over fields [11–13]. In recent years, with the rapid development of China's agricultural aviation, plant protection UAVs (unmanned aerial vehicles), which are an important part of agricultural aviation, have been widely studied and employed [14]. Compared to manned aircrafts, the advantages of UAVs include ease of control, ability to fly at low altitudes, lack of requirement for specific takeoff or landing space, good maneuverability, being lightweight, and low maintenance costs [15–18]. In contrast, UAV spraying technology is much more efficient, safe and flexible.

The aerial atomizer is the most important component of UAV application, which directly affects the spray effectiveness of plant protection UAVs. According to various atomization methods, the commonly used atomizers for UAV applications mainly include pressure and centrifugal forms. The performance parameters, features and applications are shown in Table 1. It has been found that the efficiency of UAV spraying still needs to be improved because of its uneven distribution of droplet deposition and high risk of drift, which causes serious environmental pollution and significant pesticide residues [19–22]. The atomizer's atomization performance, primarily involving droplet size, droplet spectrum width and effective swath width, directly affects droplet deposition distribution and drift [23]. The droplets of a large size tend to be deposited, while the droplets of a small size tend to drift [24]. Droplets with a narrow droplet spectral width will reduce the ratio of maximum and minimum droplets, which means it is easier to control droplet deposition and reduce droplet drift [25]. The speed variation in the centrifugal atomizer has been studied for site-specific management in distribution with prescription maps in precision agriculture [26]. The centrifugal atomizer is widely used in aerial spraying because of its controllable droplet size [27]. Therefore, optimizing the centrifugal atomizer's structural parameters to obtain a narrow droplet spectral width can increase droplet deposition and reduce drift. Clarifying the coupling relationship between atomizer spray parameters and atomization performance can provide reliable support for the development of implementation strategies for precision spraying, improving spraying quality and reducing pesticide consumption. In a study of centrifugal-atomizer structure, Kumar and Sarkar studied the atomization principle of slotted discs using a high-speed camera imaging technique and found that slotted discs can achieve narrow-spectrum, wide-droplet distribution even at high flow rates, as its slots can help to guide the liquid flow on the disc surface [28]. Craig et al. studied the atomization of a rotary atomizer using high-speed photography and laser droplet-sizing instrumentation, and found that the existing rotary-cage atomizer outer edge of the points or pins could increase the uniformity of droplet size [27]. Zhou et al. optimized the structure of the rotating cup atomizer based on the testing of droplet-volume median diameter and droplet spectral width, and studied the effect of the atomizer's structural parameters on its atomization performance [25]. In a centrifugal-atomizer performance study, Hooper and Spurgin studied the influence of rotation speed and flow rate on the droplet particle size of a wind-wheel-drive cage atomizer using a laser particle-size analyzer under wind-tunnel conditions [29]. Wang et al. used the response surface method to study the effect of centrifugal nozzle parameters on atomization performance [30]. Studies have shown that the droplet volume-median diameter (VMD) and the effective swath width (ESW) of an atomizer directly affect its spraying quality. In different operating environments and target crops, centrifugal atomizers require precise spraying control models to achieve the precise control of diseases and pests during aerial applications [31,32]. Some research has focused on the optimization of rotation speed and flow rate based on the existing centrifugal atomizer, while other research has focused on optimizing the centrifugal

atomizer's structural parameters with a fixed rotation speed and flow rate. However, at different rotation speeds and flow rates, the atomizer's structural parameter optimization and atomization performance models have not been studied systematically, which results in poor stability of the centrifugal-atomization performance, directly affecting the spraying effect.

**Table 1.** Classification, performance parameters and applications of commonly used atomizers for UAV applications.

Atomization Method	Description	Spray Angle	Volume Median Diameter	Features	Applications	References
Pressure form	Hollow cone nozzle	80°	Fine	Atomization good even with low pressure	Post-emergence touch herbicides, fungicides and insecticides	[33–35]
	Plain fan nozzle	80°/110° 90°/120°	Fine	Different types equipped with different operational needs: anti-drift, air-absorbing, extended range and wide-angle type	General applications	
Centrifugal form	Rotary disk	Indeterminate	Adjustable	Relatively controllable droplet size, nearly uniform atomization at high speeds, and independent control of atomization quality and flow rate	Plant protection UAVs	[25,36]

This study firstly introduces a dual-centrifugal atomizer structure developed by our team. The main structure is based on the structure of an existing slotted rotating-disc centrifugal atomizer, with a toothed rotating ring coaxially set on the outer side of the rotating disc, which rotates in the opposite direction to the rotating disc for secondary atomization [37]. Secondly, we used a laser particle-size analyzer to test the indicators of the droplet VMD and SRW in a wind tunnel with windless conditions. The effect of the above-mentioned rotating ring's structural parameters (tooth number and tooth shape) and spray parameters (rotation speed and flow rate) on VMD and SRW was studied by conducting the single-factor test, Plackett–Burman test and Box–Behnken test, and the regression models of VMD and SRW were obtained. Then, this atomizer's optimized structural parameters were obtained in combination with the post-hoc multiple comparison method. Thirdly, the effect of the optimized atomizer's spray parameters (rotation speed, flow rate and spray height) on its effective swath width (ESW) was further analyzed by conducting the Box–Behnken test, and the regression model of ESW was obtained. Optimization of the structure of the aerial dual-atomization centrifugal atomizer can provide a reference for improving the effectiveness of UAV aerial spraying. The regression models of VMD, SRW and ESW can provide a reference for controlling atomization effects and developing assignment plans for UAV aerial spraying.

## 2. Structure of Centrifugal Atomizer

In this study, we designed an aerial dual-atomization centrifugal atomizer. This atomizer differs from the rotating-disc atomizer, as an atomizer with a toothed rotating ring is coaxially set on the outer side of the slotted rotating disc which rotates in the opposite direction to the rotating disc for secondary atomization. Its main structure consists of a motor, a bevel gear commutator, a slotted rotating disc, a rotating disc flange, a toothed

rotating ring and a pipeline (Figure 1a). The motor shaft is the power source for the input gear of the bevel gear commutator, passing through its clearance-fitted output gear and the rotating-disc flange, and the toothed rotating ring was fixed at its end. The rotating disc flange is fixed to the commutator output gear. The input gear and the rotating ring rotate clockwise driven by the motor shaft, and the output gear drives the rotating disc to rotate counterclockwise. This centrifugal atomizer achieves the reverse rotation of the slotted rotating disc and the toothed rotating ring by the above working principle. The liquid is transported to the slotted rotating disc through the pipeline. Then, under the centrifugal force of the rotating disc, the liquid is fired into the rotating ring, which is hit to form more uniform droplets. The atomization process is shown in Figure 1b. The slotted-rotating-disc diameter was 83 mm. The toothed-rotating-ring diameter was 97 mm, the tooth size was  $1.3 \text{ mm} \times 2.5 \text{ mm} \times 8.2 \text{ mm}$ , the number of teeth was 64, and the tooth shape was square. In the following optimization and study, the change in the atomizer structure was on the basis of the reference atomizer structure. The rotation speed of the atomizer was the motor speed.

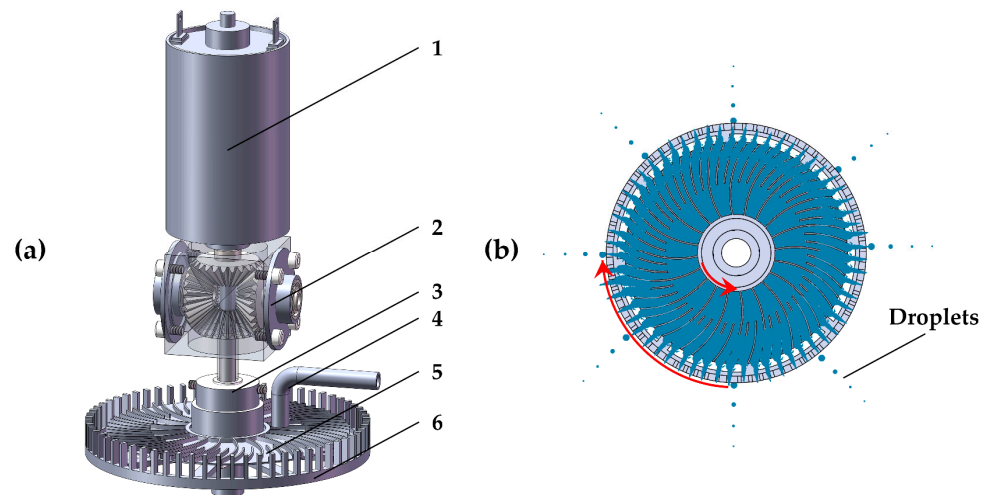


**Figure 1.** (a) Main structure of centrifugal atomizer (1. motor, 2. bevel gear commutator, 3. rotating disc flange, 4. pipeline, 5. slotted rotating disc, 6. toothed rotating ring); (b) schematic diagram of the centrifugal atomizer atomization process.

### 3. Materials and Methods

To optimize the structure of the centrifugal atomizer and study its atomization performance, the droplet characteristics of the centrifugal atomizer were tested under wind-tunnel windless conditions, and the spray width of the centrifugal atomizer was tested in the laboratory under windless conditions.

#### 3.1. Atomization Performance Evaluation

In this paper, the data used to analyze droplet characteristics included: D10, D50 or VMD, D90, and SRW; the effective swath width (ESW) of the atomizer was an indicator of the atomizer's spray width. Dn is the droplet diameter ( $\mu\text{m}$ ), which represents the sum of the volume of the given size and below, accounting for n % of the total droplet volume of the sample, and the droplet volume median diameter (VMD or D50) can be used to characterize the droplet diameter. The droplet spectral width (SRW), a dimensionless parameter, is used to indicate the degree of differential droplet-size distribution concentration (Equation (1)); the narrower the SRW, the higher the uniformity of the drop size distribution is. The effective swath width (ESW) of the atomizer indicates the distance from the atomizer's lead hammer point as the center of the circle to the spray width (cm) corresponding to D50 (the deposition volume is accumulated to 50% of that direction). Different droplet

sizes are suitable for different biological targets [32]. ESW is used to plan rational routes for aerial spraying [38].

$$SRW = \frac{D90 - D10}{D50} \quad (1)$$

### 3.2. Test Equipment and Method

In this study, the droplet-size test experiment was conducted in the wind-tunnel lab, located in the National Center for International Collaboration Research on Precision Agricultural Aviation Pesticide Spraying Technology (NPAAC) in South China Agricultural University, Guangzhou, China, built according to the international standard ISO2856-2012. It can generate airspeeds of 2–51 m/s and the test section size is 2.0 m × 1.1 m × 20.0 m (width × height × length) (Figure 2a). The wind tunnel is the first high–low speed compound wind tunnel dedicated to agricultural aviation in China and one of the most advanced wind tunnels in worldwide agricultural engineering. To test the droplet size of the centrifugal atomizer, the test equipment consisted of a spraying system and a droplet-size testing system. The DP-02 laser particle-size analyzer (OMC instrument co. LTD, Zhuhai, China) was used in the test section to measure the droplet size. This laser particle-size analyzer is capable of measuring droplets in the range of 1 to 1500 µm. The laser particle-size analyzer consists of a collimated laser generator, a signal-acquisition device and a data-processing system. The distance between the laser transmitter and receiver is 2.0 m. In the test, the laser particle-analyzer outputs were D50, D10, D90 and the particle-size differential distribution curve. According to the ASABE (S572.3) standard, droplet-size measurement must ensure that a representative, cross-sectional sample of the spray plume is achieved to obtain the droplet-size spectrum, and the distance between the atomizer and the measurement point should be between 200 mm and 500 mm to reduce contamination of the laser lens [39]. It is assumed that the droplet-size spectrum is uniformly distributed in the spray plume and that any cross-section is completely representative of the droplet distribution of the deposition ring; therefore, only one cross-sectional sample of the centrifugal-atomizer spray plume was measured in the test. Specifically, the laser particle-size analyzer was placed 30 cm below the atomizer, the droplets were ejected horizontally by the atomizer and the laser beam passed through its atomization area (Figure 3a). The spraying system consisted of a centrifugal atomizer with 48v DC power, a diaphragm pump with 30v DC power and several pipelines (Figures 2b and 3b). By changing the input voltage of the two powers, the rotation speed (600–7000 r/min) of the centrifugal atomizer and the flow rate (500–1000 mL/min) of the pump, respectively, were controlled.

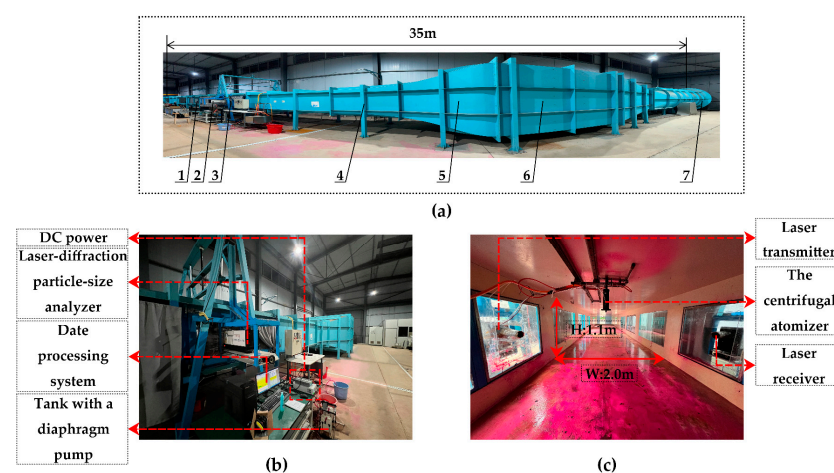


**Figure 2.** Wind tunnel used in the droplet-size test experiment. (a) Form and structure (1. observation window, 2. droplet-size testing system, 3. test section, 4. mounting bracket, 5. contractive segment, 6. steady section, 7. drive section); (b,c), the droplet test system and spraying system.



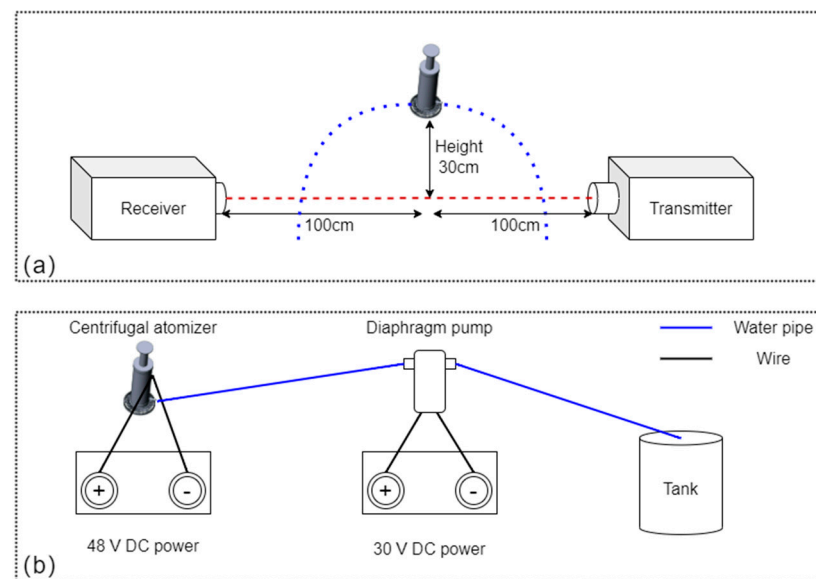


**Figure 3.** Schematic diagram of the droplet testing system (a) and spraying system (b).

The centrifugal-atomizer spray-width test was conducted in the laboratory under windless conditions (Figure 4). The droplet collection boxes were placed in eight directions below the atomizer (east, southeast, south, southwest, west, northwest, north and northeast). Under windless conditions, there were no droplets in the central part of the deposition area of the centrifugal atomizer; therefore, no droplet collection box was placed in the central area. Due to the large number of tasks for collecting and weighing droplets, 9.3 cm × 9.3 cm square plastic boxes were used. The spraying system was the same as that of the above droplet-size test. The spray height (1–3 m) was controlled by the lifting rod of the atomizer's support stand. For each test group, after atomizer spraying for 3 min, the outside of each box was wiped using dry towels, and then the droplet mass of each box was weighed. Finally, according to the droplet distribution, the spray width corresponding to D50 in each direction was calculated, and the ESW of each group was obtained as its average value of eight directions.

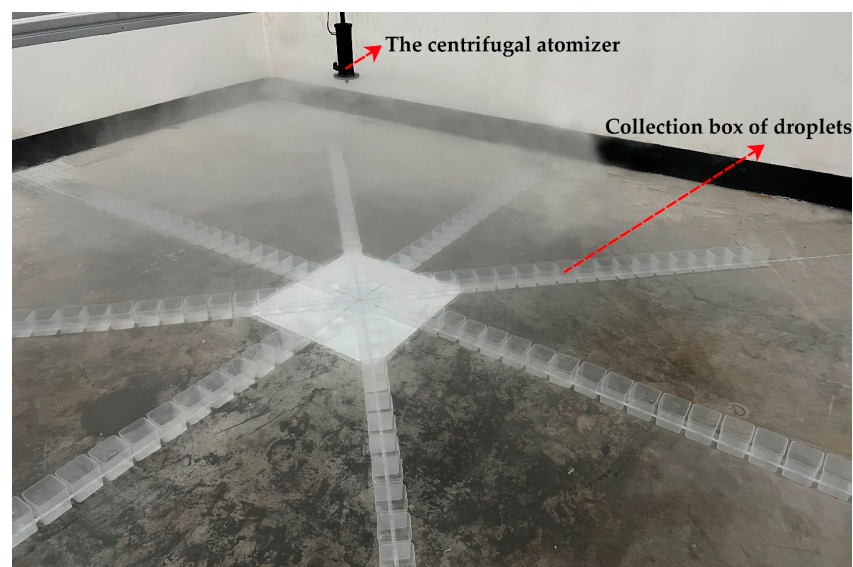


**Figure 4.** Scheme of spray-width test experiment.

### 3.3. Droplet Characteristics Test of Atomizer

In this work, the factors that have a significant effect on VMD and SRW, and their numerical intervals, were initially obtained by combining the single-factor test and Plackett–Burman test. Then, the structure of the atomizer was optimized by combining the Box–Behnken response surface method and post-hoc multiple comparison method, and the regression models of VMD and SRW were obtained. The specific experimental design is as follows.

#### 3.3.1. Single-Factor Test of Droplet Characteristics

We studied the effects of four factors—the rotation speed of the centrifugal atomizer ( $X_1$ ), flow rate ( $X_2$ ), tooth number of the rotating ring ( $X_3$ ), and tooth shape of the rotating ring ( $X_4$ )—on the VMD and SRW of the centrifugal atomizer by conducting single-factor tests. According to the structural design of the toothed rotating ring and pre-test, the tooth number was set between 0 and 128 (Figure 5a), and the tooth shape was selected from wedge, square and semicircular shapes (Figure 5b). Although the UAV pump flow rate varied from 5.5 to 0.25 L/min (for all atomizers), the centrifugal atomizers are generally ultra-low-volume ones; therefore, the tested flow rate was set to be from 500 to 1000 mL/min [40,41]. The required droplet size for aerial spraying is 50–300  $\mu\text{m}$ , with the combination of the pre-test, the rotation speed was set to be from 600 to 7000 r/min [42]. The fixed parameters used in the single-factor test were a rotation speed of 4000 r/min, flow rate of 700 mL/min, tooth number of 64, and square tooth shape. The specific factors and levels are shown in Table 2. Each test group was repeated three times. The results of this test can obtain a range of levels for each factor to be used in subsequent tests.

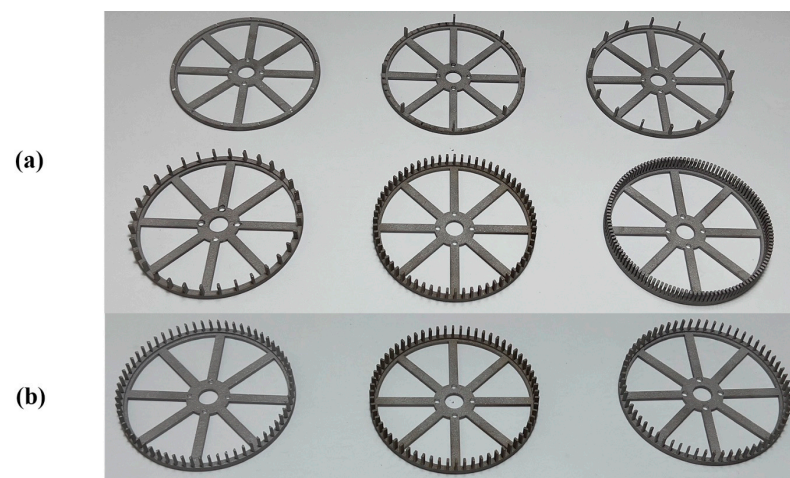


**Figure 5.** Rotating rings with different tooth numbers (a) and different tooth shapes (b).

**Table 2.** Factors and levels of single-factor design.

Factors	Level Values
$X_1$ : Rotation speed (r/min)	600, 2000, 3000, 4000, 5000, 6000, 7000
$X_2$ : Flow rate (mL/min)	500, 600, 700, 800, 900, 1000
$X_3$ : Tooth number	0, 8, 16, 32, 64, 128
$X_4$ : Tooth shape	wedge, square, semicircular

#### 3.3.2. Plackett–Burman Test of Droplet Characteristics

The Plackett–Burman test is an experimental design method which can be used to determine the significance of each factor. Four factors ( $X_1$ : rotation speed of centrifugal atomizer,  $X_2$ : flow rate,  $X_3$ : tooth number of rotating ring,  $X_4$ : tooth shape of rotating ring) were screened in this test. Three levels of  $-1$ ,  $0$  and  $+1$  were taken for each factor; the ends

of the levels in the single-factor test were selected as the levels of +1 and −1, respectively; the average of the two ends was taken as the level of 0 and the response values were droplet VMD and SRW. The specific coding levels are shown in Table 3.

**Table 3.** Factors and levels for the Plackett–Burman design.

Factors	Level Values	
	−1	1
X <sub>1</sub> : Rotation speed (r/min)	600	7000
X <sub>2</sub> : Flow rate (mL/min)	500	1000
X <sub>3</sub> : Tooth number	0	128
X <sub>4</sub> : Tooth shape	wedge	square

### 3.3.3. Box–Behnken Test of Droplet Characteristics

Box–Behnken tests were carried out on the basis of the factors that had a significant effect on VMD and SRW in the Plackett–Burman test above. The factors include X<sub>1</sub>: rotation speed of centrifugal atomizer, X<sub>2</sub>: flow rate and X<sub>3</sub>: tooth number of rotating ring, and the response values were droplet VMD and SRW. The specific coding levels are shown in Table 4.

**Table 4.** Factors and levels for the Box–Behnken design of droplet characteristics.

Factors	Level Values		
	−1	0	1
X <sub>1</sub> : Rotation speed (r/min)	600	3800	7000
X <sub>2</sub> : Flow rate (mL/min)	500	750	1000
X <sub>3</sub> : Tooth number	8	20	32

### 3.4. Spray-Width Test of Atomizer

In addition to the droplet characteristics, the spray width is another important indicator which affects the quality of aerial spraying, which plays an important role in the route planning of UAV spraying. In this test, according to the test results of Section 3.3, the optimized centrifugal atomizer was selected to proceed with the Box–Behnken response surface test which has three factors: rotation speed of centrifugal atomizer (X<sub>1</sub>), flow rate (X<sub>2</sub>) and spray height (X<sub>3</sub>), and the response value was the atomizer ESW. The coding levels are shown in Table 5.

**Table 5.** Factors and levels for the Box–Behnken design of spray-width Test.

Factors	Level Values		
	−1	0	1
X <sub>1</sub> : Rotation speed (r/min)	600	3800	7000
X <sub>2</sub> : Flow rate (mL/min)	500	750	1000
X <sub>3</sub> : Spray height (m)	1	2	3

## 4. Results

### 4.1. Centrifugal-Atomizer Droplet-Characteristics Test

#### 4.1.1. Single-Factor Test Results of Droplet Characteristics

A series of single-factor tests were conducted to initially determine the effect of each test factor on droplet VMD and SRW, and the results are shown in Figure 6. Figure 6a shows the effect of the rotation speed of centrifugal atomizer (X<sub>1</sub>) on VMD and SRW. As X<sub>1</sub> gradually increased from 600 r/min to 7000 r/min, VMD decreased from 315.22 µm to 52.44 µm and SRW decreased from 2.10 to 0.61. Within the range of X<sub>1</sub> of 600 to 7000 r/min, the decrease rate of VMD was great when X<sub>1</sub> was less than 2000 r/min, and the decrease



trend of VMD gradually tended to smooth when  $X_1$  exceeded 2000 r/min. The increase in rotation speed leads to the decrease in VMD and SRW. Figure 6b shows the effect of flow rate ( $X_2$ ) on VMD and SRW, as  $X_2$  increased from 500 mL/min to 1000 mL/min, VMD increased from 62.33  $\mu\text{m}$  to 74.3  $\mu\text{m}$  and SRW increased from 0.79 to 1.4. An increase in flow rate leads to an increase in VMD and SRW. Figure 6c shows the effect of the rotating ring's tooth number ( $X_3$ ) on VMD and SRW. As  $X_3$  increased from 0 to 16, VMD decreased from 198.19 to 64.81  $\mu\text{m}$  and SRW decreased from 1.03 to 0.6. Then, as  $X_3$  continued to increase from 16 to 128, VMD gradually increased to 94.33 and SRW gradually increased to 1.7. As  $X_3$  increased, both VMD and SRW decreased and then increased, and both achieved the minimum value when  $X_3$  was 16. As  $X_3$  increased from 8 to 128, VMD was smaller than  $X_3$  at 0, and as  $X_3$  increased from 8 to 64, SRW was smaller than  $X_3$  at 0, indicating that the teeth of the toothed rotating ring may play a role in the atomization process in secondary atomization, allowing the atomizer to produce droplets with smaller droplet particle size and greater uniformity. However, as  $X_3$  increased from 16 to 128, the teeth gradually filled the circumference of the rotating ring, the droplet size became larger and the droplet uniformity decreased, which indicates that a gradually decreasing tooth gap may prevent the full secondary atomization of the fluid from the rotating disc. Figure 6d shows the effect of the rotating ring's tooth shape ( $X_4$ ) on the VMD and SRW. The VMD and SRW of the droplets produced by the wedge tooth shape were 89.05  $\mu\text{m}$  and 1.1, the VMD and SRW of the droplets produced by the square tooth shape were 68.94  $\mu\text{m}$  and 1.01, and the VMD and SRW of the droplets produced by the semicircular tooth shape were 90.32  $\mu\text{m}$  and 1.05. The droplet VMD and SRW produced by the square tooth shape were smaller than the wedge and semicircular tooth shapes, which indicates that the square tooth shape has better atomization capability.

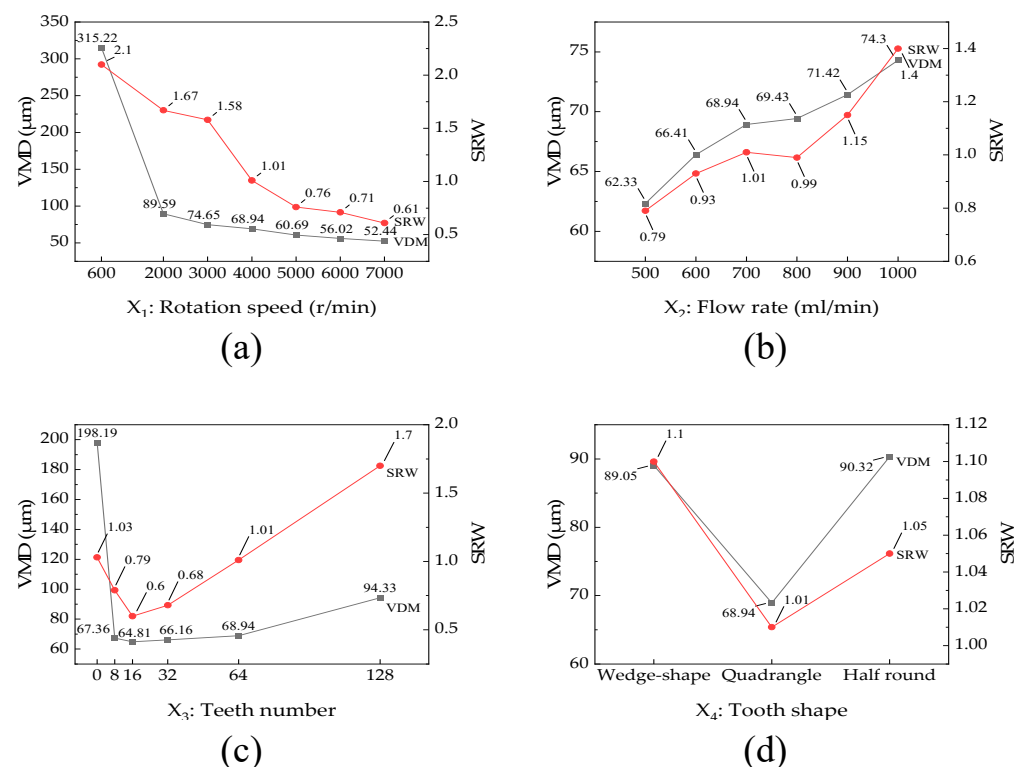


**Figure 6.** Results of single-factor tests on the effect of rotation speed (a), flow rate (b), tooth number (c) and tooth shape (d) on the droplet volume median diameter (VMD) and spectral width (SRW).

#### 4.1.2. Screening for Important Factors Affecting Droplet Characteristics Using the Plackett–Burman Design

The Plackett–Burman test was designed using the Design-Expert 11 software. The VMD and SRW results of the 18 test schemes and the four factors are shown in Table 6.

**Table 6.** Plackett–Burman test protocol and results.

Test Serial Number	Test Factors				VMD ( $\mu\text{m}$ )	SRW
	$X_1$	$X_2$	$X_3$	$X_4$		
1	−1	1	1	1	541.16	1.35
2	0	0	0	−1	95.6	0.99
3	0	0	0	−1	95.4	1.02
4	0	0	0	1	72.46	1.79
5	0	0	0	1	70.92	1.68
6	−1	−1	−1	−1	920.38	0.63
7	1	−1	1	1	89.46	0.99
8	0	0	0	1	70.96	1.62
9	−1	1	1	−1	574.59	1.59
10	−1	−1	1	−1	356.33	1.87
11	−1	1	−1	1	951.64	0.59
12	1	1	−1	1	128.71	0.8
13	−1	−1	−1	1	932.19	0.61
14	0	0	0	−1	93.61	0.98
15	1	1	−1	−1	128.36	0.78
16	1	−1	1	1	88.53	0.95
17	1	−1	−1	−1	116.89	0.73
18	1	1	1	−1	87.18	0.83

In order to analyze the significance of the effect of the test factors on test indicators, the analysis module of the Design-Expert 11 software was used to analyze the variance of the test results. The results of the significance analysis for each factor are shown in Table 7. As can be seen from the table, the rotation speed ( $X_1$ ), flow rate ( $X_2$ ) and tooth number ( $X_3$ ) had a significant effect on VMD ( $p < 0.01$ ), and tooth shape ( $X_4$ ) had no significant effect on VMD ( $p > 0.05$ ). The order of test factors affecting VMD was: rotation speed ( $X_1$ ) > tooth number ( $X_3$ ) > flow rate ( $X_2$ ) > tooth shape ( $X_4$ ); the rotation speed ( $X_1$ ) and tooth number ( $X_3$ ) had a significant effect on SRW ( $p < 0.01$ ), and flow rate ( $X_2$ ) and tooth shape ( $X_4$ ) had no significant effect on SRW ( $p > 0.05$ ). The order of the factors affecting SRW was: tooth number ( $X_3$ ) > rotation speed ( $X_1$ ) > tooth shape ( $X_4$ ) > flow rate ( $X_2$ ). Therefore, the factors of rotation speed ( $X_1$ ), flow rate ( $X_2$ ) and tooth number ( $X_3$ ) were selected as the three factors for the Box–Behnken test, and the insignificant factor of tooth shape was taken as square tooth shape.

**Table 7.** Significance analysis of Plackett–Burman test results.

Factors	VMD ( $\mu\text{m}$ )				SRW			
	Sum of Squares	Degree of Freedom	F-Value	p-Value	Sum of Squares	Degree of Freedom	F-Value	p-Value
$X_1$	0.0112	1	2341.72	<0.0001	0.2107	1	4.3	0.0623
$X_2$	0.0104	1	8.26	0.0151	0.0007	1	0.0138	0.9086
$X_3$	0.0000	1	146.04	<0.0001	1.07	1	21.94	0.0007
$X_4$	$4.968 \times 10^{-6}$	1	1.12	0.3133	0.1027	1	2.10	0.1755
$R^2 = 0.9956$ ; Adj $R^2 = 0.9941$ ; C.V. % = 2.55%; Adeq Precision = 67.31					$R^2 = 0.7118$ ; Adj $R^2 = 0.6070$ ; C.V. % = 20.12%; Adeq Precision = 8.9077			

Note:  $p \leq 0.01$  (highly significant);  $0.01 < p \leq 0.05$  (significant).

#### 4.1.3. Box–Behnken Test of Droplet Characteristics

The Box–Behnken test for droplet characteristics designed using Design-Expert 11 software had a total of 17 testing spots in the scheme, which included 12 analysis factors and five zero-point estimation errors. The test design scheme and response values of VMD and SRW are shown in Table 8.

**Table 8.** Scheme and results of droplet characteristics Box–Behnken test.

Test Serial Number	Test Factors			VMD (μm)	SRW
	X <sub>1</sub>	X <sub>2</sub>	X <sub>3</sub>		
1	0	0	0	73.39	0.86
2	−1	−1	0	301.66	2.08
3	0	−1	1	64.47	0.83
4	−1	0	−1	450.96	1.52
5	0	0	0	73.44	0.82
6	0	1	−1	82.23	0.92
7	1	1	0	55.34	0.6
8	0	0	0	73.06	0.82
9	1	−1	0	46.99	0.63
10	−1	0	1	295.18	2.07
11	1	0	1	52.69	0.59
12	0	0	0	74.42	0.78
13	0	0	0	73.32	0.8
14	0	−1	−1	66.48	1.13
15	−1	1	0	356.7	1.75
16	1	0	−1	56.68	0.71
17	0	1	1	78.64	0.89

#### 1. Significance analysis and regression model

The quadratic regression models of VMD and SRW were obtained by analyzing the Box–Behnken test results using Design-Expert 11 software. The ANOVA results of the quadratic regression models are shown in Table 9. Here,  $p$ -values < 0.01 for the VMD and SRW regression models indicated that the regression equations for VMD and SRW were highly significant. The  $p$ -values for lack of fit were 0.0705 and 0.0878 (>0.05), respectively, indicating that the actual fit and the regression equation had a small proportion of abnormal errors and were well-fitted. The variation coefficients CV were 2.21% and 4.63%, respectively, indicating good test reliability. The determination coefficients,  $R^2$ , were 0.9976 and 0.9770, respectively, and the calibration determination coefficients, Adj  $R^2$ , were 0.9945 and 0.9474, respectively, indicating good reliability of the regression equation. The Adeq precision results were 53.2 and 17.47, respectively, indicating good accuracy of the regression model. Therefore, the developed models can be regarded as a reliable representative of the experimental results. In addition, all primary terms,  $X_1$ ,  $X_2$  and  $X_3$ , and secondary terms,  $X_1^2$  and  $X_3^2$ , had a significant effect on VMD, and the other terms had no significant effect on VMD. The primary term,  $X_1$ , and secondary terms,  $X_1^2$  and  $X_3^2$ , had a significant effect on SRW, and the remaining terms had no significant effect on SRW. After fitting the regression to the experimental results, the regression equations of VMD and SRW with rotation speed ( $X_1$ ), flow rate ( $X_2$ ) and tooth number ( $X_3$ ) as variables were obtained as shown in Equations (2) and (3), respectively.

$$\frac{1}{\text{Sqrt}(\text{VMD})} = 0.045988 + 0.000031X_1 - 0.000046X_2 + 0.001153X_3 - 1.04691E - 09X_1X_2 - 3.84255E - 08X_1X_3 + 8.03871E - 08X_2X_3 - 2.19177E - 09X_1^2 + 1.89852E - 09X_2^2 - 0.000021X_3^2 \quad (2)$$

$$\frac{1}{\text{Sqrt}(\text{SRW})} = -0.161108 + 0.000143X_1 + 0.00155X_2 + 0.02511X_3 - 3.34486E - 08X_1X_2 + 1.24818E - 06X_1X_3 + 9.45843E - 06X_2X_3 - 7.29405E - 09X_1^2 - 7.6503E - 07X_2^2 - 0.000539X_3^2 \quad (3)$$

**Table 9.** Significance analysis of droplet characteristics Box–Behnken test results.

Source	VMD ( $\mu\text{m}$ )				SRW			
	Sum of Squares	Degree of Freedom	F-Value	p-Value	Sum of Squares	Degree of Freedom	F-Value	p-Value
Model	0.0162	9	319.63	<0.0001	0.7153	9	33.05	<0.0001
$X_1$	0.0138	1	2441.38	<0.0001	0.6297	1	261.81	<0.0001
$X_2$	0.0002	1	34.23	0.0006	0.0037	1	1.54	0.2545
$X_3$	0.0001	1	9.17	0.0192	0.0016	1	0.6808	0.4365
$X_1X_2$	$2.806 \times 10^{-6}$	1	0.4976	0.5033	0.0029	1	1.19	0.3113
$X_2X_3$	$8.709 \times 10^{-6}$	1	1.54	0.2540	0.0092	1	3.82	0.0915
$X_1X_3$	$2.326 \times 10^{-7}$	1	0.0413	0.8448	0.0032	1	1.34	0.2851
$X_1^2$	0.0021	1	376.16	<0.0001	0.0235	1	9.77	0.0167
$X_2^2$	$5.928 \times 10^{-6}$	1	1.05	0.3393	0.0096	1	4.00	0.0855
$X_3^2$	0.0000	1	7.08	0.0325	0.0254	1	10.55	0.0141
Residual	0.0000	7			0.0168	7		
Lack of Fit	0.0000	3	5.30	0.0705	0.0130	3	4.58	0.0878
Pure Error	$7.936 \times 10^{-6}$	4			0.0038	4		
Cor Total	0.0163	16			0.7321	16		
$R^2 = 0.9976$ ; Adj $R^2 = 0.9945$ ; C.V. % = 2.21%; Adeq Precision = 53.2					$R^2 = 0.9770$ ; Adj $R^2 = 0.9474$ ; C.V. % = 4.63%; Adeq Precision = 17.47			

Note:  $p \leq 0.01$  (highly significant);  $0.01 < p \leq 0.05$  (significant).

## 2. Response surface analysis

The response surface plots of VMD and SRW and the corresponding contour plots are shown in Figure 7. Each response surface plot represents the effect of two independent variables with the values of the other variables kept at the 0 level; the shape of the corresponding contour plot indicates whether the interaction between the independent variables was significant. The interactions of rotation speed ( $X_1$ ) and flow rate ( $X_2$ ), rotation speed ( $X_1$ ) and tooth number ( $X_3$ ), and flow rate ( $X_2$ ) and tooth number ( $X_3$ ) on VMD are shown in Figure 7a–c, respectively; the interactions of rotation speed ( $X_1$ ) and flow rate ( $X_2$ ), rotation speed ( $X_1$ ) and tooth number ( $X_3$ ), and flow rate ( $X_2$ ) and tooth number ( $X_3$ ) on SRW are shown in Figure 7d–f, respectively.

Combined with Figure 7a,d, from a transverse perspective, when  $X_2$  was constant, VMD and SRW decreased with increasing  $X_1$ . The smaller  $X_2$  was, the faster VMD and SRW decreased during the increase in  $X_1$ . In addition, from the longitudinal perspective, when  $X_1$  was constant, the VMD gradually increased, while the SRW first decreased and then increased with increasing  $X_2$ .

Combined with Figure 7b,e, from the transverse perspective, when  $X_3$  was constant, VMD and SRW decreased as  $X_1$  increased. From the longitudinal perspective, when  $X_1$  was constant, VMD and SRW first decreased and then increased as  $X_3$  increased.

Combined with Figure 7c,f, from the transverse perspective, when  $X_3$  was constant, VMD increased and SRW first decreased and then increased as  $X_2$  increased. From the longitudinal perspective, when  $X_2$  was constant, both VMD and SRW decreased and then increased as  $X_3$  increased.

In general, as the atomizer's rotation speed increases, the droplet size becomes smaller and more uniform. As the flow rate increases, the droplet size becomes larger and less uniform. The toothed-rotating-ring-assisted atomization can obviously make the droplet size smaller and more uniform. However, when the tooth number is too large, the droplet characteristics become worse; this may be because it is difficult for the liquid to pass through the dense tooth gap, resulting in inadequate secondary atomization. Therefore,



the selection of the right number of teeth is the key to optimizing the structure of the dual-atomization centrifugal atomizer.

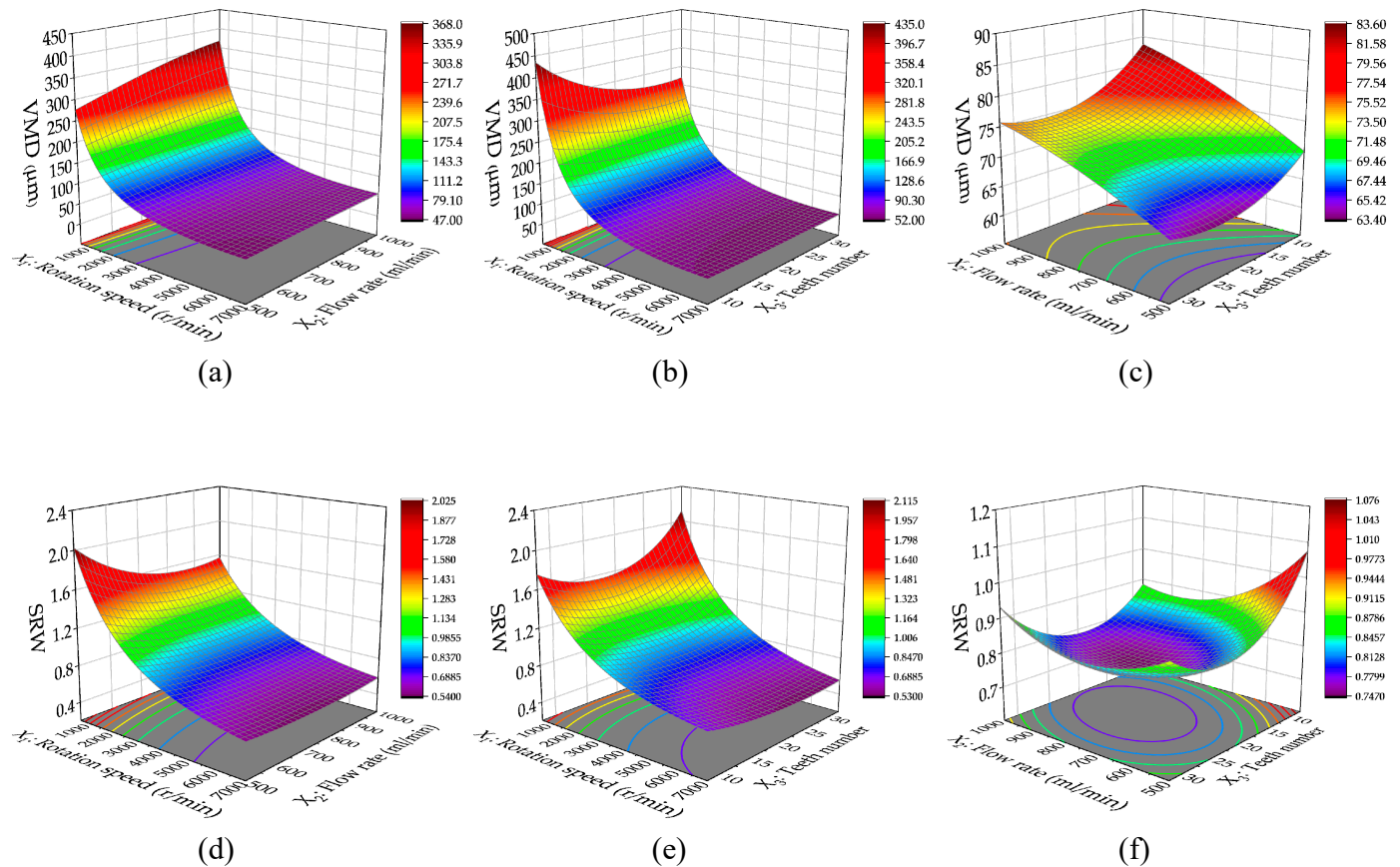


**Figure 7.** Response surface plots of each factor on VMD (a–c) and SRW (d–f).

#### 4.1.4. Structural Parameter Optimization of Atomizer

As can be seen from Figure 7b,c,e,f, the tooth number ( $X_3$ ) that achieved the lowest VMD and SRW was between 8 and 32 in the full rotation-speed ( $X_1$ ) and flow-rate ( $X_2$ ) range, but the optimal  $X_3$  was not unique for the combination of different  $X_1$  and  $X_2$ . Therefore, the least-significant-difference method was used to compare the means of the test results in Table 7 of Section 4.1.3. The VMD and SRW mean values of different  $X_3$  are shown in Figure 8. The results show that the VMD values in ascending order were 8, 32 and 20, and the SRW values in ascending order were 32, 8 and 20; thus, the optimal  $X_3$  was 20. Finally, the optimal tooth number of the toothed rotating ring was 20 and the tooth shape of the toothed rotating ring was square. The spray width of the centrifugal atomizer was studied later based on this optimal structure.

#### 4.2. Box–Behnken Test of Spray Width

There were 17 test points in the Box–Behnken test protocol for the spray-width test, including 12 analysis factors and 5 zero-point estimation errors. The test design scheme and response values of ESW are shown in Table 10.

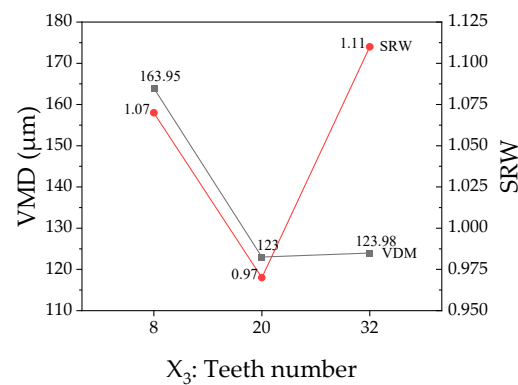


Figure 8. Graph of the VMD and SRW mean values comparison of each tooth number level.

Table 10. Scheme and results of spray width Box–Behnken test.

Test Serial Number	Test Factors			Effective Swath Width (ESW (cm))
	X <sub>1</sub>	X <sub>2</sub>	X <sub>5</sub>	
1	1	−1	0	85.24
2	−1	1	0	48.18
3	0	0	0	76.5
4	−1	0	−1	45.84
5	0	0	0	74.08
6	1	1	0	87.75
7	0	0	0	75.03
8	0	1	−1	83.35
9	1	0	−1	107.76
10	0	−1	3	73.36
11	1	0	3	87.31
12	0	0	0	73.29
13	0	−1	−1	79.74
14	−1	−1	0	43.41
15	−1	0	3	48.84
16	0	0	0	72.95
17	0	1	3	78.26

#### 4.2.1. Significance Analysis and Regression Model

The quadratic regression model was obtained by analyzing the Box–Behnken test results using Design-Expert software. Variance analysis results of the quadratic regression model are shown in Table 11. The  $p$ -values  $< 0.01$  for the ESW regression models, indicating a very significant relationship between the ESW and regression equation. The  $p$  value of lack-of-fit was 0.2409 ( $> 0.05$ ), indicating a small percentage of abnormal errors in the actual fitting and the regression equation, and a good fitting. The variation coefficient  $CV = 2.14\%$ , indicating good test reliability. The determination coefficient  $R^2 = 0.9975$  and the calibration determination coefficient  $Adj R^2 = 0.9943$ , indicating good regression equation reliability. Adeq Precision = 57.26, indicating a good precision of the regression model. In addition, all the primary terms,  $X_1$ ,  $X_2$  and  $X_5$ ; interaction terms,  $X_1X_2$ ,  $X_2X_5$ ; and secondary terms,  $X_1^2$  and  $X_5^2$  had a significant effect on ESW, and the remaining terms had no significant effects on ESW. After fitting the regression to the experimental results, the regression equations of ESW with rotation speed ( $X_1$ ), flow rate ( $X_2$ ) and spray height ( $X_5$ ) as variables was obtained, as shown in Equation (4):

$$\frac{1}{ESW} = 0.026138 - 4.99145E - 06X_1 - 6.82333E - 06X_2 + 0.002902X_3 + 6.07843E - 10X_1X_2 + 2.74496E - 07X_1X_3 - 3.1033E - 07X_2X_3 + 3.07543E - 10X_1^2 + 2.08516E - 09X_2^2 - 0.000844X_3^2 \quad (4)$$

**Table 11.** Significance analysis of spray width Box–Behnken test results.

Source	Sum of Squares	Degree of Freedom	F-Value	p-Value	
Model	0.0003	9	311.03	<0.0001	significant
$X_1$	0.0002	1	2278.16	<0.0001	
$X_2$	$2.013 \times 10^{-6}$	1	20.58	0.0027	
$X_5$	$9.143 \times 10^{-7}$	1	9.35	0.0184	
$X_1X_2$	$9.459 \times 10^{-7}$	1	9.67	0.0171	
$X_2X_5$	$3.086 \times 10^{-6}$	1	31.55	0.0008	
$X_1X_5$	$2.408 \times 10^{-8}$	1	0.2462	0.6350	
$X_1^2$	0.0000	1	426.94	<0.0001	
$X_2^2$	$7.151 \times 10^{-8}$	1	0.7311	0.4208	
$X_3^2$	$2.997 \times 10^{-6}$	1	30.64	0.0009	
Residual	$6.847 \times 10^{-7}$	7			not significant
Lack of Fit	$4.2 \times 10^{-7}$	3	2.12	0.2409	
Pure Error	$2.646 \times 10^{-7}$	4			
Cor Total	0.0003	16			

$R^2 = 0.9975$ ; Adj  $R^2 = 0.9943$ ; C.V. % = 2.14%; Adeq Precision = 57.26

Note:  $p \leq 0.01$  (highly significant);  $0.01 < p \leq 0.05$  (significant).

#### 4.2.2. Response Surface Analysis

Response surface plots of the corresponding models were generated using Design-Expert 11 software, as shown in Figure 9, demonstrating the interaction between the rotation speed,  $X_1$ ; flow rate,  $X_2$ ; and spray height,  $X_5$  on ESW.

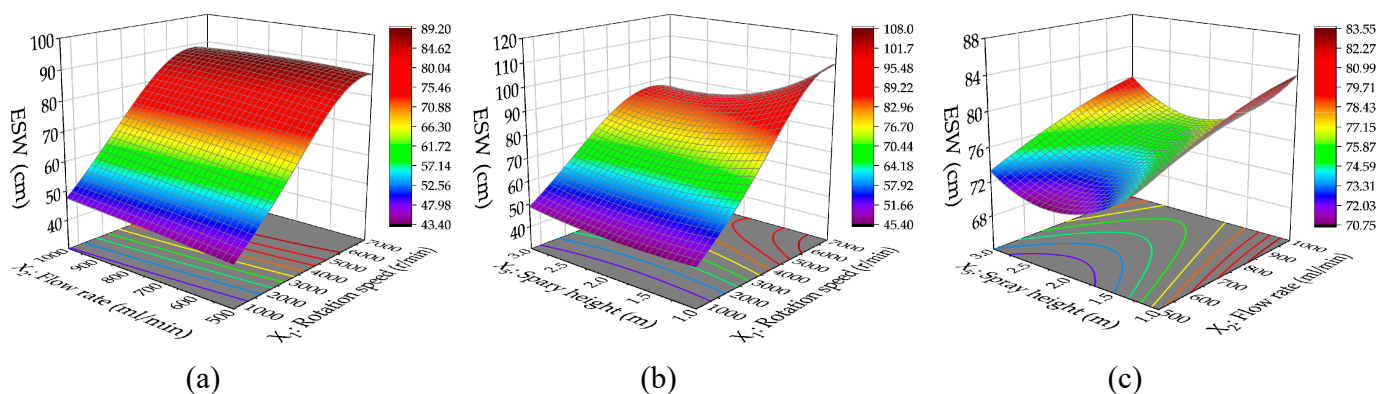


**Figure 9.** Response surface plot of rotation speed and flow rate (a), flow rate and spray height (b), rotation speed and spray height (c) on effective swath width (ESW).

Figure 9a–c show the interaction surfaces of rotation speed ( $X_1$ ) and flow rate ( $X_2$ ), rotation speed ( $X_1$ ) and spray height ( $X_5$ ), and flow rate ( $X_2$ ) and spray height ( $X_5$ ) on ESW, respectively. From Figure 9a, it can be seen that when  $X_5$  was constant, the ESW increased first and then gradually became constant as  $X_1$  increased. When  $X_1$  was constant, the ESW was positively correlated with  $X_2$ . The reason for this may be that as the atomizer's rotation speed increases, the VMD becomes smaller, and the deposition time of small droplets is longer and they are easier to drift, resulting in larger ESW. From Figure 9b, it can be seen that when  $X_2$  was constant, ESW increased first and then gradually became constant with the increase in  $X_1$ . When  $X_1$  was low, the ESW was positively correlated with  $X_5$ . When  $X_1$  was high, the ESW was negatively correlated with  $X_5$ . This may be because when the atomizer's rotation speed is high, the VMD is small, and the drift becomes serious as spray height becomes larger, which leads to the droplets becoming off-target, making the ESW smaller. When the atomizer's rotation speed is low, the VMD is larger and the droplets move in the air for a longer time as spray height increases, resulting in larger ESW. As can

be seen from Figure 9c, when  $X_1$  was constant, the ESW showed a trend of first decreasing and then increasing with the increase in  $X_5$ . When  $X_5$  was constant, ESW was positively correlated with  $X_2$ . The reason for this may be that as the atomizer's flow rate increases, although the particle size becomes larger, the speed of the droplets leaving the atomizer becomes faster, therefore resulting in a larger ESW.

When the ESW becomes larger, the UAV needs to fly at a wider row spacing to prevent heavy spray; when the ESW becomes smaller, the UAV needs to fly at narrower row spacing to prevent missed spray. In general, the rotation speed, flow rate and spray height have certain effects on the ESW of the atomizer, and the predicted ESW of the above regression model can provide a reference for the setting of row spacing in the UAV spraying process.

## 5. Conclusions

In this paper, the structural optimization of the dual-atomization centrifugal atomizer and its atomization performance were studied. First, the ANOVA concluded that the rotation speed, flow rate, and tooth number had a significant effect on the droplet VMD and SRW. Although the tooth shape had no significant effect on the droplet VMD and SRW, probably due to the variability in the recorded values, the square tooth shape had the smallest droplet VMD and the narrowest droplet SRW; thus, the square tooth shape had the best atomization effect among the three tooth shapes. By correctly combining tooth shape and tooth number, a dual-atomization centrifugal atomizer with optimized structure can be obtained. The optimized structure parameters were obtained as a square tooth shape and tooth number of 20. Then, the regression models of the droplet VMD and SRW were obtained using the response surface method, and the determination coefficients  $R^2$  were 0.9976 and 0.9770, respectively; thus, these models can be used to accurately control the precise spray effect of the optimized dual-atomization centrifugal atomizer.

In order to study the spray width of the dual-atomization centrifugal atomizer, the effects of the rotation speed, flow rate and spray height on the ESW of the atomizer were studied. The experimental results showed that the rotation speed, flow rate, and spray height had a significant effect on the atomizer's ESW. Therefore, the rotation speed, flow rate and spray height need to be comprehensively considered during the UAV spraying. The regression model of the atomizer's ESW was obtained using the response surface method, and the determination coefficient  $R^2$  was 0.9975, which indicated that the regression model is accurate; thus, the model can be used to predict and control the ESW of the atomizer during the UAV spraying.

Zhou et al. optimized the structure of the rotating-cup atomizer with a fixed rotation speed (3600 r/min) and flow rate (700 mL/min) [25]. Ru et al. optimized the rotation-speed and flow-rate parameters of a centrifugal atomizer with 80mm rotating-disc diameter [43]. Yang et al. tested the volume median diameter and effective swath width of an aviation-special centrifugal atomizer in an indoor windless environment, and established the mathematical model of volume median diameter and effective swath width [38]. Compared with previous research, this study proposed an aerial dual-atomization centrifugal-atomizer structure, and further studied the atomization-performance modeling base on the structure optimization of this atomizer. Moreover, the test results indicate that the atomization effect of this atomizer structure is better than a slotted-rotary-disc atomizer.

The limitation of this work is that we tested the droplet characteristics and atomizer-spray swath under windless conditions, and, therefore, did not consider the impact of ambient wind and downwash airflow. The main reason is that ambient wind cannot be precisely controlled and downwash airflow is affected by many factors and cannot be accurately simulated. Although the downwash airflow affects the droplet deposition in many cases, it has almost no effect on the droplet characteristics of atomizers. Furthermore, the centrifugal atomizers could be used not only for UAVs but also for other vehicles such as tractors, ATVs (all-terrain vehicles) or UTVs (utility terrain vehicles). Therefore, in future research, this optimized atomizer will be equipped on a UAV to study the field spraying performance.



Overall, this work provided an optimized dual-atomization centrifugal atomizer for efficient UAV aerial application, and the established regression model of atomization performance can provide a reference for the control of precise aerial application.

### Abbreviation

The following abbreviations are used in this manuscript:

UAV	unmanned aerial vehicle
VMD	volume median diameter
SRW	spectral width
ESW	effective swath width
FAO	UN Food and Agriculture Organization
NPAAC	National Center for International Collaboration Research on Precision Agricultural Aviation Pesticide Spraying Technology
ATV	all-terrain vehicle
UTV	utility terrain vehicle

**Author Contributions:** Conceptualization, J.D. and X.X.; methodology, J.Y. and X.X.; software, J.Y.; validation, J.Y., Z.Y. and J.D.; formal analysis, J.Y.; investigation, J.Y. and G.H.; resources, Z.Y. and J.D.; data curation, J.Y.; writing—original draft preparation, J.Y.; writing—review and editing, Z.Y. and X.X.; visualization, J.Y.; supervision, J.D.; project administration, Z.Y. and X.X.; funding acquisition, Z.Y. All authors have read and agreed to the published version of the manuscript.

**Funding:** This research was supported by the Laboratory of Lingnan Modern Agriculture Project (NT2021009), and the China Agriculture Research System of MOF and MARA (CARS-31). This support is greatly acknowledged.

**Institutional Review Board Statement:** Not applicable.

**Informed Consent Statement:** Not applicable.

**Data Availability Statement:** The data presented in this study are available on request from the corresponding author.

**Conflicts of Interest:** The authors declare no conflict of interest.

### References

1. FAO. *The Future of Food and Agriculture: Trends and Challenges*; FAO: Rome, Italy, 2017. Available online: <http://www.fao.org/3/a-i6583e.pdf> (accessed on 27 December 2022).
2. Maes, W.H.; Steppe, K. Perspectives for Remote Sensing with Unmanned Aerial Vehicles in Precision Agriculture. *Trends Plant Sci.* **2019**, *24*, 152–164. [[CrossRef](#)] [[PubMed](#)]
3. Cheng, Z.; Qi, L.; Cheng, Y. Cherry Tree Crown Extraction from Natural Orchard Images with Complex Backgrounds. *Agriculture* **2021**, *11*, 431. [[CrossRef](#)]
4. Ji, X.; Wang, A.; Wei, X. Precision Control of Spraying Quantity Based on Linear Active Disturbance Rejection Control Method. *Agriculture* **2021**, *11*, 761. [[CrossRef](#)]
5. Wang, G.; Han, Y.; Li, X.; Andaloro, J.; Chen, P.; Hoffmann, W.C.; Han, X.; Chen, S.; Lan, Y. Field evaluation of spray drift and environmental impact using an agricultural unmanned aerial vehicle (UAV) sprayer. *Sci. Total Environ.* **2020**, *737*, 139793. [[CrossRef](#)] [[PubMed](#)]
6. Cao, L.; Cao, C.; Wang, Y.; Li, X.; Zhou, Z.; Li, F.; Yan, X.; Huang, Q. Visual Determination of Potential Dermal and Inhalation Exposure Using Allura Red As an Environmentally Friendly Pesticide Surrogate. *ACS Sustain. Chem. Eng.* **2017**, *5*, 3882–3889. [[CrossRef](#)]
7. Meng, Y.; Song, J.; Lan, Y.; Mei, G.; Liang, Z.; Han, Y. Harvest aids efficacy applied by unmanned aerial vehicles on cotton crop. *Ind. Crops Prod.* **2019**, *140*, 111645. [[CrossRef](#)]
8. Creech, C.F.; Henry, R.S.; Werle, R.; Sandell, L.D.; Hewitt, A.J.; Kruger, G.R. Performance of Postemergence Herbicides Applied at Different Carrier Volume Rates. *Weed Technol.* **2015**, *29*, 611–624. [[CrossRef](#)]
9. Lamichhane, J.R.; Dachbrodt-Saaydeh, S.; Kudsk, P.; Messéan, A. Toward a Reduced Reliance on Conventional Pesticides in European Agriculture. *Plant Dis.* **2016**, *100*, 10–24. [[CrossRef](#)]
10. Meng, Y.; Lan, Y.; Mei, G.; Guo, Y.; Song, J.; Wang, Z. Effect of aerial spray adjuvant applying on the efficiency of small unmanned aerial vehicle for wheat aphids control. *Int. J. Agric. Biol. Eng.* **2018**, *11*, 46–53. [[CrossRef](#)]
11. Williamson, J.R.; Neilsen, W.A. influence of forest site on rate and extent of soil compaction and profile disturbance of skid trails during ground-based harvesting. *Can. J. For. Res.* **2000**, *30*, 1196–1205. [[CrossRef](#)]

12. Braunack, M.V.; Johnston, D.B. Changes in soil cone resistance due to cotton picker traffic during harvest on Australian cotton soils. *Soil Tillage Res.* **2014**, *140*, 29–39. [CrossRef]
13. Gemtos, T.A.; Chouliaras, N.; Marakis, S. Vinasse Rate, Time of Application and Compaction Effect on Soil Properties and Durum Wheat Crop. *J. Agric. Eng. Res.* **1999**, *73*, 283–296. [CrossRef]
14. Zhang, D.; Lan, Y.; Chen, L.; Wang, X.; Liang, D. Current Status and Future Trends of Agricultural Aerial Spraying Technology in China. *Trans. Chin. Soc. Agric. Mach.* **2014**, *45*, 53–59. Available online: <https://kns.cnki.net/kcms/detail/detail.aspx?FileName=NYJX201410009&DbName=CJFQ2014> (accessed on 3 December 2022).
15. Yang, S.; Yang, X.; Mo, J. The application of unmanned aircraft systems to plant protection in China. *Precis. Agric.* **2017**, *19*, 278–292. [CrossRef]
16. Guo, S.; Li, J.; Yao, W.; Zhan, Y.; Li, Y.; Shi, Y. Distribution characteristics on droplet deposition of wind field vortex formed by multi-rotor UAV. *PLoS ONE* **2019**, *14*, e220024. [CrossRef] [PubMed]
17. Bae, Y.; Koo, Y.M. Flight Attitudes and Spray Patterns of a Roll-Balanced Agricultural Unmanned Helicopter. *Appl. Eng. Agric.* **2013**, *29*, 675–682. [CrossRef]
18. Lan, Y.; Hoffmann, W.C.; Fritz, B.K.; Martin, D.E.; Lopez, J.D., Jr. Spray drift mitigation with spray mix adjuvants. *Appl. Eng. Agric.* **2008**, *1*, 5–10. [CrossRef]
19. Hilz, E.; Vermeer, A.W.P. Spray drift review: The extent to which a formulation can contribute to spray drift reduction. *Crop Prot.* **2013**, *44*, 75–83. [CrossRef]
20. Qiu, B.; Wang, L.; Cai, D.; Wu, J.; Ding, G.; Guan, X. Effects of flight altitude and speed of unmanned helicopter on spray deposition uniform. *Trans. Chin. Soc. Agric. Eng.* **2013**, *29*, 25–32. Available online: <https://kns.cnki.net/kcms/detail/detail.aspx?FileName=NYGU201324004&DbName=CJFQ2013> (accessed on 3 December 2022).
21. He, X. Improving severe dragging actuality of plant protection machinery and its application techniques. *Trans. Chin. Soc. Agric. Eng.* **2004**, *20*, 13–15. Available online: <https://kns.cnki.net/kcms/detail/detail.aspx?FileName=NYGU200401003&DbName=CJFQ2004> (accessed on 3 December 2022).
22. Doruchowski, G.; Świechowski, W.; Masny, S.; Maciesiak, A.; Tartanus, M.; Bryk, H.; Hołownicki, R. Low-drift nozzles vs. standard nozzles for pesticide application in the biological efficacy trials of pesticides in apple pest and disease control. *Sci. Total Environ.* **2017**, *575*, 1239–1246. [CrossRef] [PubMed]
23. Zhang, S.; Qiu, B.; Xue, X.; Sun, T.; Peng, B. Parameters optimization of crop protection UAS based on the first industry standard of China. *Int. J. Agric. Biol. Eng.* **2020**, *13*, 29–35. [CrossRef]
24. Liu, X.; Zhou, H.; Zhen, J. Research advances of the technologies for spray drift control of pesticide application. *Trans. Chin. Soc. Agric. Eng.* **2005**, *21*, 186–190. Available online: <https://kns.cnki.net/kcms/detail/detail.aspx?FileName=NYGU200501042&DbName=CJFQ2005> (accessed on 3 December 2022).
25. Zhou, Q.; Xue, X.; Qin, W.; Cai, C.; Zhou, L. Optimization and test for structural parameters of UAV spraying rotary cup atomizer. *Int. J. Agric. Biol. Eng.* **2017**, *10*, 78. [CrossRef]
26. Romano, E.; Schillaci, G.; Longo, D.; Bisaglia, C.; Failla, S. Purpose-Intended Modification of a Conventional Sprayer Machine for Application in Precision Agriculture. *Saf. Health Welf. Agric. Agro-Food Syst.* **2022**, *252*, 327–336. [CrossRef]
27. Craig, I.P.; Hewitt, A.; Terry, H. Rotary atomiser design requirements for optimum pesticide application efficiency. *Crop Prot.* **2014**, *66*, 34–39. [CrossRef]
28. Kumar, P.; Sarkar, S. Experimental investigation of liquid disintegration on slotted disc in centrifugal atomization process. *Chem. Eng. Res. Des.* **2019**, *145*, 76–84. [CrossRef]
29. Hooper, G.H.S.; Spurgin, P.A. Droplet size spectra produced by the atomization of a ULV formulation of fenitrothion with a Micronair AU5000 rotary atomizer. *Crop Prot.* **1995**, *14*, 27–30. [CrossRef]
30. Wang, D.; Xu, S.; Li, Z.; Cao, W. Analysis of the Influence of Parameters of a Spraying System Designed for UAV Application on the Spraying Quality Based on Box–Behnken Response Surface Method. *Agriculture* **2022**, *12*, 131. [CrossRef]
31. Washington, J.R. Relationship between the Spray Droplet Density of Two Protectant Fungicides and the Germination of *Mycosphaerella fijiensis* Ascospores on Banana Leaf Surfaces. *Pestic. Sci.* **1997**, *50*, 233–239. [CrossRef]
32. Uk, S. Tracing Insecticide Spray Droplets by Sizes on Natural Surfaces. The State of the Art and its Value. *Pestic. Sci.* **1977**, *8*, 501–509. [CrossRef]
33. Jiao, Y.; Xue, X.; Ding, S. Research status and prospects of spraying performance of spray nozzles. *Trans. Chin. Agric. Mech.* **2021**, *42*, 40–50+56. Available online: <http://www.cnki.com.cn/Article/CJFDTOTAL-GLJH202112007.htm> (accessed on 22 January 2023).
34. ASAE. Droplet Size Classification of Aerial Application Nozzles. ANSI/ASAE S641 (FEB2022). 2022. Available online: <https://elibrary.asabe.org/abstract.asp?aid=48958> (accessed on 22 January 2023).
35. He, Y.; Xiao, S.; Fang, H.; Dong, T.; Tang, Y.; Nie, P.; Wu, J.; Luo, S. Development situation and spraying decision of spray nozzle for plant protection UAV. *Trans. Chin. Soc. Agric. Eng.* **2018**, *13*, 113–124. Available online: <https://www.cnki.com.cn/Article/CJFDTOTAL-NYGU201813014.htm> (accessed on 22 January 2023).
36. Lefebvre, H.; McDonell, V.G. *Atomization and Sprays*, 2nd ed.; CRC Press: Boca Raton, FL, USA, 2017; pp. 7–8.
37. Yang, Z.; Yu, J.; Xu, X.; Duan, J.; Ou, Y.; Shen, D.; Tan, X.; Wu, B.; Cai, L.; Zeng, Z.; et al. A Centrifugal Atomization Nozzle. 2021. Available online: <https://kns.cnki.net/kcms/detail/detail.aspx?FileName=CN113385316A&DbName=SCPD2021> (accessed on 28 December 2022).

38. Yang, F.; Xue, X.; Cai, C.; Zhou, Q.; Sun, Z. Atomization Performance Test and Influence Factors of Aviation Special Centrifugal Nozzle. *Trans. Chin. Soc. Agric. Mach.* **2019**, *50*, 96–104. Available online: <http://kns.cnki.net/KCMS/detail/detail.aspx?FileName=NYJX201909011&DbName=CJFQ2019> (accessed on 16 January 2023).
39. ASAE. Spray Nozzle Classification by Droplet Spectra. ANSI/ASAE S572.3 (FEB2020). 2020. Available online: <https://elibrary.asabe.org/abstract.asp?aid=51101> (accessed on 2 December 2022).
40. Hanif, A.S.; Han, X.; Yu, S.H. Independent Control Spraying System for UAV-Based Precise Variable Sprayer: A Review. *Drones* **2022**, *6*, 383. [CrossRef]
41. Fan, Q. The Research on the Pesticide Spray System Using for the Mini Unmanned Helicopter. Master's Thesis, Nanjing Forestry University, Nanjing, China, 2011. Available online: <https://kns.cnki.net/kcms/detail/detail.aspx?FileName=1011401249.nh&DbName=CMFD2012> (accessed on 4 February 2023).
42. CAAC. Quality Indexes of Agricultural Aviation Operation-Part 1: Spraying Operation. MH/T 1002.1-2016. 2016. Available online: <https://hbba.sacinfo.org.cn/stdDetail/e8993d4d62653dc7eaa6dd22500412d4> (accessed on 4 February 2023).
43. Ru, Y.; Jia, Z.; Fan, Q.; Che, J. Remote Control Spraying System Based on Unmanned Helicopter. *Trans. Chin. Soc. Agric. Mach.* **2012**, *43*, 47–52. Available online: <http://www.cnki.com.cn/Article/CJFDTotol-NYJX201206010.htm> (accessed on 16 January 2023).

**Disclaimer/Publisher's Note:** The statements, opinions and data contained in all publications are solely those of the individual author(s) and contributor(s) and not of MDPI and/or the editor(s). MDPI and/or the editor(s) disclaim responsibility for any injury to people or property resulting from any ideas, methods, instructions or products referred to in the content.